Volume 1 | Number 1 | Jan 2013 | Pages 1–100

ChemComm

Chemical Communications
www.rsc.org/chemcomm

ROYAL SOCIETY OF CHEMISTRY

ROYAL SOCIETY OF CHEMISTRY

www.rsc.org/chemcomm

ChemComm

COMMUNICATION

Facet-Dependent NiS$_2$ polyhedrons on counter electrodes for dye-sensitized solar cells

Jinlong Zheng, Wei Zhou *, Yiran Ma, Wei Cao, Chengbo Wang, and Lin Guo *

Octahedral and cubic NiS$_2$ nanocrystals enclosed by {111} and {100} planes were separately used as counter electrodes (CEs) incorporated into a Pt-free dye-sensitized solar cells (DSSCs). The DSSC assembled by NiS$_2$ octahedrons exhibited a conversion efficiency of 5.98%, better than that by NiS$_2$ cubes (5.43%). DFT calculations indicate the better catalytic effect could be ascribed to higher surface energy, more active sites, and more suitable adsorption energy of {111} planes compared with the {100} planes.

Although dye-sensitized solar cells (DSSCs), one kind of clean, low-cost and easily-fabricated cells, have developed in labs for decades, their commercialization still necessitates further improvements.[1, 2] As an important component in the DSSC, the counter electrode (CE) mediates regeneration of the sensitizer after electron injection, playing a key role in catalysing the reduction of the electrolyte.[3, 4] The conventional Pt CEs have remarkably high conductivity and efficient catalysis on the reduction of I$_3^-$ to I$^-$. However, their high cost and limited reserves restrict the extensive commercial application of DSSCs.[5-7] Thus, much effort has been devoted to develop high-efficient, low-cost and naturally abundant non-Pt catalysts. Recently, metal sulphides electrodes such as Co$_9$S$_8$, FeS$_2$, SnS$_2$ and MoS$_2$ have showed potential application to replace Pt CEs.[8-11] Compared to other semiconductor materials, nickel sulphides including various compounds such as NiS, Ni$_3$S$_2$ and NiS$_2$, have superior electrocatalytic activity and excellent electrical conductivity.[12-14] For example, the nanocomposites of NiS$_2$ NPs and reduced graphene oxide sheets (NiS$_2$@RGO) used as CEs of DSSCs showed higher conversion efficiency than Pt.[15] It has been verified that the NiS$_2$ shows obvious catalytic properties towards I$_3^-$/I$^-$.[14, 15]

Semiconductor nano- or microcrystals with different facets usually exhibit different catalytic activities and photovoltaic performance as the particular surface atomic arrangement and unsaturated dangling bonds. For example, serving as CE in DSSC, Bi$_2$S$_3$ microflowers assembled by one-dimension sheets grown along the <130> direction showed better electrical conductivity and conversion efficiency than those with 1D sheet along the <211> axis.[16] Although various sulphide nanomaterials were used as CEs in DSSCs, the influence of

different surfaces of the NiS$_2$ polyhedrons on the properties of DSSCs were rarely studied. Herein, we reported a simple hydrothermal method for the synthesis of uniform NiS$_2$ octahedrons and cubes with similar sizes (the detail of the experiment seen in ESI†). Using these two kinds of nanocrystals as CEs, the influence of exposed different facets on the performance was carefully studied and we found NiS$_2$ octahedrons composed by outer surfaces of (111) showed better performance than cubes enclosed by (100) facets.
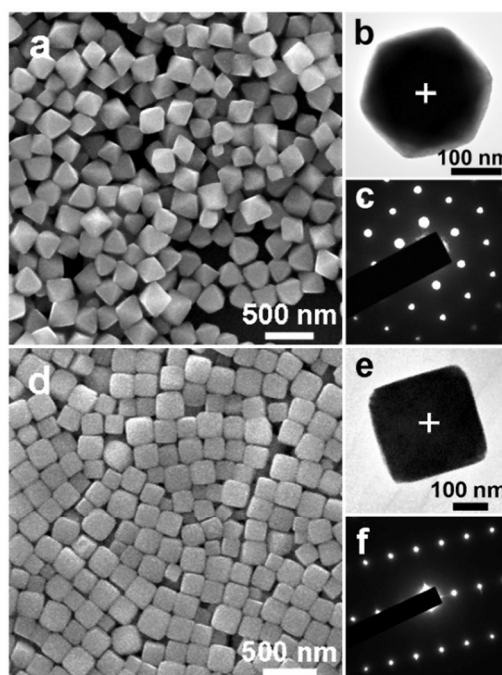
Fig. 1 Characterization of SEM, TEM, and SAED on NiS$_2$ octahedrons (a, b, and c) and cubes (d, e, and f). SAED patterns (c and f) were obtained from the corresponding particles with the electron beam along the [111] and [001] directions as marked in Fig. 1b and 1e, respectively.
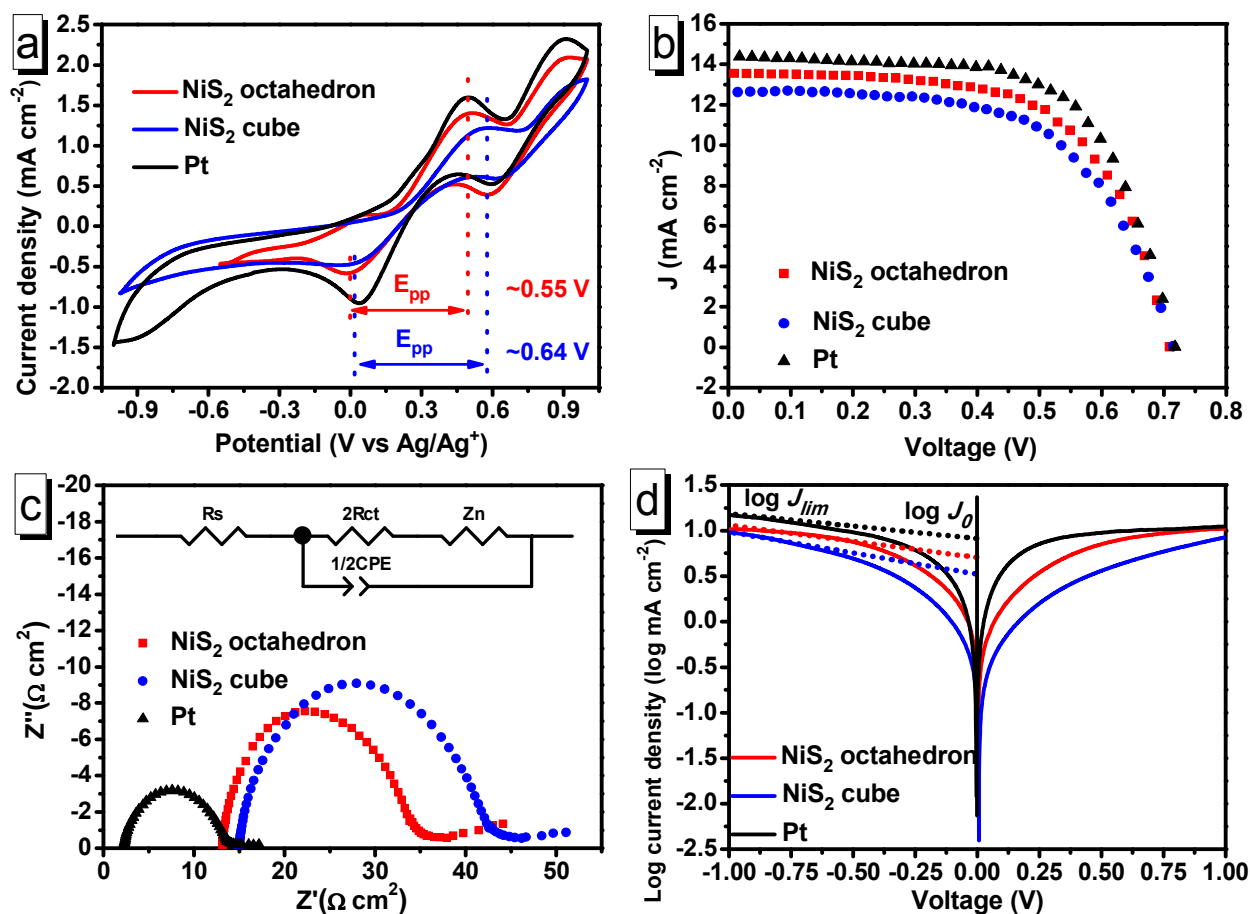
Fig. 2 (a) CV curves of the I_3^-/I^- redox for NiS_2 octahedrons, NiS_2 cubes and Pt CEs; (b) *J-V* characteristics of DSSCs with different CEs under simulated AM1.5G solar light (100 mW cm^{-2}); Nyquist plots (c) and Tafel polarization curves (d) of DSSCs by different CEs.

The morphology of the octahedrons and cubes were shown in Fig. 1. XRD patterns of the polyhedrons in Fig. S1 showed they were in good agreement with the component of NiS_2 (JCPDS No. 11-0099). As shown in Fig. 1a and 1d, uniform NiS_2 octahedrons and cubes with an average size of ~250 nm were well dispersed. Typical TEM images for NiS_2 octahedron and cube were shown in Fig. 1b and Fig. 1e. Their corresponding selected-area electron diffraction (SAED) patterns in Fig. 1c and Fig. 1f suggested a good single-crystal characteristic of the NiS_2 and confirmed their crystal facets of (111) and (100). The similar patterns of FeS_2, which had the same space group as NiS_2, had been reported by other researchers.[17, 18] The extra diffraction spots marked by red circles in SAED patterns, such as (1 -1 0), (1 0 -1) and (0 1 -1) in Fig. S2a and (0 1 0) in Fig. S2b, came from the secondary diffraction of the crystals (detailed analysis seen in ESI†).

To investigate the performance of different CEs, cyclic voltammetry (CV), *J-V* characteristics, electrochemical impedance spectroscopy (EIS) and Tafel polarization were carried out and the results were shown in Fig. 2a-d. The detailed photovoltaic and EIS parameters were summarized in Table 1. As electrocatalyst for DSSCs, its catalytic activity was crucially important for improving the performance of the cell. To characterize the electrocatalytic activity of various catalysts, CV curves were obtained and shown in Fig. 2a. The left pair could be assigned to the redox reaction of I_3^-/I^- and the right one assigned to the reaction of I_2/I_3^-.[8, 19] The peak-to-peak separation (E_{pp}) between the left pair was inversely correlated

with the rate of the I_3^-/I^- redox reaction.[20, 21] The E_{pp} value and the peak current were considered as two important parameters to determine the catalytic performances of different CEs. Higher peak current and lower E_{pp} value indicated a better electrocatalytic capability toward the I_3^-/I^- redox reduction for DSSCs.[4, 21] As shown in Fig. 2a, the octahedrons exhibited higher peak current density (~1.40 mA cm^{-2}) and lower E_{pp} (~0.55 V) compared to the cubes (~1.22 mA cm^{-2}, ~0.64 V), showing a better electrocatalytic activity.

Fig. 2b showed the photocurrent density-voltage (*J-V*) curves of the DSSCs with NiS_2 octahedrons, cubes and Pt CEs. All DSSCs had similar open circuit voltage (VOC, ~715 mV), and the reason was that these DSSCs had the same photoanode and the electrolyte. The NiS_2 octahedron CE revealed higher short-circuit photocurrent density (J_{sc} = 13.55 mA cm^{-2}) and fill factor (FF = 0.62) than that of cube CE (12.62 mA cm^{-2}, 0.60), resulting in a higher power conversion efficiency (PCE). The enhanced J_{SC} values originated from high catalytic activity for the I_3^- reduction demonstrated by high peak current and low E_{pp} from CV measurement.[7] The improvement of FF could be attributable to the lower R_s and R_{ct} from the EIS tests.[22, 23] The DSSC based on octahedrons produced a PCE of 5.98% (up to 91% of Pt), higher than that of cubes (5.43%). The better performance of the octahedrons could be ascribed to the $\{111\}_{NiS2}$ planes, having higher surface energy, more suitable adsorption energy, and more catalytic active sites than the $\{100\}$ planes, which was confirmed by theoretical calculation later.

Table 1 Photovoltaic and electrochemical impedance parameters of the DSSCs assembled with various CEs.

CE	V_{OC} (mV)	J_{SC} (mA cm^{-2})	FF	η (%)	R$_s$ (Ω cm^2)	R$_{ct}$ (Ω cm^2)	C (μF)
Pt	718	14.37	0.63	6.55	2.24	6.25	48.53
NiS$_2$-cube	715	12.62	0.60	5.43	14.98	13.17	29.44
NiS$_2$-octahedron	712	13.55	0.62	5.98	13.14	9.86	39.15

The EIS analysis was performed using symmetric cells fabricated by two identical CEs with the structure of the CE/electrolyte/CE. The Nyquist plots of DSSCs with symmetric CEs were shown in Fig. 2c. The ohmic series resistance (R$_s$) could be obtained from the high-frequency intercept on the real axis containing the sheet resistance of the counter electrode and the electrolyte. The R$_s$ of the NiS$_2$ octahedron CE was 13.14 $\Omega \cdot$cm^2, smaller than that of the cubes (14.98 $\Omega \cdot$cm^2), which revealed a better electrical conductivity of the octahedron CE. The semicircle in high frequency region occurred from the charge-transfer resistance (R$_{ct}$), which was a measure of electron exchange between the counter electrode and the electrolyte, changing inversely with the catalytic activity of different CEs on the reduction of triiodide.[21] The R$_{ct}$ of the NiS$_2$ octahedron CE (9.86 $\Omega \cdot$cm^2) was smaller than that of the cubes (13.17 $\Omega \cdot$cm^2), revealing the octahedrons with {111} facets had better catalytic activity than cubes with {100} facets.[21, 24] The low frequency corresponded to the Nernst diffusion impedance (Z$_N$) of the I$_3^-$/I$^-$ redox couple in the electrolyte.[25] Constant phase element (CPE) values were obtained from the EIS spectrum and NiS$_2$ octahedron CE exhibited a larger capacitance (C, 39.15 μF) than that of NiS$_2$ cube CE (29.44 μF) indicating a higher surface area of the electrodes, which was responsible for higher PCE.[24, 26] The resistance results revealed the octahedrons had better electrical conductivity and catalytic properties compared with cubes. Besides, the resistivity of NiS$_2$ polyhedrons was also investigated by a four-probe resistivity tester. The results indicated that NiS$_2$ octahedrons (0.31 $\Omega \cdot$cm) exhibited better electrical conductivity than cubes (0.35 $\Omega \cdot$cm) in line with the EIS analysis (Table S1, ESI†).

Fig. 2d showed the Tafel polarization curves. The intersection of the cathodic branch and the equilibrium potential line (black solid line) could be considered as the exchange current density (log J_0), which could also be calculated by the equation, $J_0 = RT/nFR_{ct}$, where R is the gas constant, T is the temperature, n is the number of electrons involved in the reduction, F is the Faraday's constant and R$_{ct}$ is the charge-transfer resistance extracted from the EIS spectra (Figure 2c) (calculated values seen in Table S2).[27] The J_0 values of the different CEs calculated from equation are nearly the same as that calculated values from Tafel polarization curves. Apparently, Fig. 2d showed higher J_0 value of octahedrons than that of cubes, indicating the octahedron CE exhibited a better electrochemical performance in the catalytic reduction of I$_3^-$.

The catalytic properties of NiS$_2$ samples are controlled by five steps including diffusion (Step 1 and 5), catalysis (Step 3), and adsorption/desorption (Step 2 and 4) as shown in Fig. 3a. As I$_3^-$ ions are bulkier than I$^-$ ions with lower concentration in the iodide-based liquid electrolyte, Step 1 of the I$_3^-$ diffusion towards the catalyst (CE) becomes the control factor of the diffusion.[28] As for the adsorption/desorption process, they are apparently controlled by adsorption energy of NiS$_2$ polyhedrons. Step 3 shows the catalytic reduction of I$_3^-$ to I$^-$ ions on NiS$_2$

facets relating to their surface energy. As the intention is to study the influence of the different surfaces of polyhedron CEs, we focus Steps 3, 4, and 5 concerning surfaces of polyhedrons. Density functional theory (DFT) calculations were employed to disclose deeply the difference of the {111} and {100} facets by calculating their surface energy and adsorption energy. The crystal structure of the NiS$_2$ was illustrated in Fig. S3. It has a space group symmetry of Pa-3, with Ni atoms occupying the sites in the face-centered cubic sublattice while the sulfur dimers centering about the anion positions.
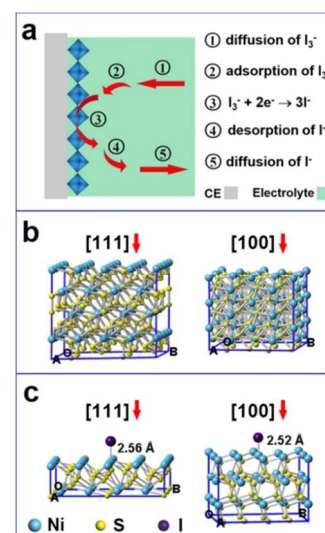
Fig. 3 (a) Schematic of the catalytic process on CEs including five steps. Perspective views of the crystal structures for surface energy (b) and adsorption energy calculation (c) on NiS$_2$ with the (111) and the (100) planes. The top layers showed the exposed Ni atoms in (111) and (100) planes. Ni-I bond distances, d(Ni-I), were 2.56 Å away from the (111) and 2.52 Å from the (100) plane.

Fig. 3b showed the model used to calculate the surface energy for the {111} and {100} facets of NiS$_2$. The calculation showed that the surface energy for the {111} facet was estimated to be 1.94 J m^{-2}, which was higher than that for the {100}$_{NiS2}$ (~1.58 J m^{-2}). We could also find the {111} facet of FeS$_2$ (the same crystal structure as NiS$_2$) had higher surface energy than the {100} facet.[29] The result indicated that the {111} facets were more active and had better catalysis (faster Step 3) than the {100} facets.

The adsorption energies of iodine atom (E$_{ad}^I$) simulation models were shown in Fig. 3c (the calculations seen in Fig. S6). For triiodide reduction reaction, too high E$_{ad}^I$ limited the overall activity due to the difficulty in iodine removal, while too weak

adsorption hindered iodine molecular dissociation.[1] The adsorption energy at the CH_3CN/electrode interface ranging from ~0.33 to 1.20 eV was thought to be a good descriptor for the iodine reduction activity.[30, 31] The {111} and {100} facets were estimated to be 0.98 eV and 1.49 eV of E_{ad}^I, respectively. The suitable E_{ad}^I of the {111} facets increases the adsorption/desorption rate, and thus leads to faster electron transfer, resulting in higher conversion efficiency of the octahedron CE. Besides, the {111} facet has more exposed Ni atoms than the {100} facet in the models as marked by red arrows in Fig. S4b and S5b. As proved by other reports, nickel has catalytic property towards I_3^-/I^-,[32] which might also be the active elements in the nickel sulfides for catalyzing I_3^-/I^-. To sum up, $\{111\}_{NiS2}$ facet with higher surface energy and more suitable adsorption energy, shows a better catalytic property towards I_3^-/I^- compared with the $\{100\}_{NiS2}$ facet. Therefore, the octahedron CE provides a faster electron transfer and improved electrochemical properties of the DSSCs than the cube CE.

In summary, octahedral and cubic NiS_2 with exposed {111} and {100} surfaces have been successfully synthesized by a facile hydrothermal method. Studies on their electrocatalytic properties reveal that the as-prepared NiS_2 nanocrystals exhibit interesting facet-dependent effect as CEs in DSSCs. The octahedral NiS_2 exhibits a conversion efficiency of 5.98% higher than that assembled with cubic NiS_2 (5.43%). DFT calculations of surface energy suggest that the $\{111\}_{NiS2}$ facets exhibit a higher surface energy and more active sites than the {100} facets. It would improve the reduction rate of I_3^- to I^- in the catalytic process. Calculations of adsorption energy suggest that the {111} facets present more suitable adsorption energy than the {100} facets with better I_3^- adsorption and I^- removal. The models show the $\{111\}_{NiS2}$ facets have more exposed Ni atoms than the $\{100\}_{NiS2}$ facets, which might provide improved catalytic active sites towards I_3^-/I^-. The facet-dependent effect would provide a probable route to improve the properties of non-Pt CEs in DSSCs by designing nanostructures with optimal crystal planes.

Notes and references

School of Chemistry and Environment, Beihang University, Beijing 100191, China. E-mail: zhouwei@buaa.edu.cn; guolin@buaa.edu.cn; Tel (Fax): +86-10-82316066

1. Y. Li, H. Wang, H. Zhang, P. Liu, Y. Wang, W. Fang, H. Yang, Y. Li and H. Zhao, *Chemical communications*, 2014, **50**, 5569-5571.
2. M. Gratzel, *Nature*, 2001, **414**, 338-344.
3. X. Chen, Y. Hou, B. Zhang, X. H. Yang and H. G. Yang, *Chemical Communications*, 2013, **49**, 5793-5795.
4. E. B. Bi, H. Chen, X. D. Yang, W. Q. Peng, M. Gratzel and L. Y. Han, *Energy & Environmental Science*, 2014, **7**, 2637-2641.
5. Q. Chang, L. Huang, J. Wang, Z. Ma, P. Li, Y. Yan, J. Zhu, S. Xu, L. Shen, Q. Chen, Q. Yu and W. Shi, *Carbon*, 2015, **85**, 185-193.
6. C.-T. Lee, J.-D. Peng, C.-T. Li, Y.-L. Tsai, R. Vittal and K.-C. Ho, *Nano Energy*, 2014, **10**, 201-211.
7. L. X. Yi, Y. Y. Liu, N. L. Yang, Z. Y. Tang, H. J. Zhao, G. H. Ma, Z. G. Su and D. Wang, *Energy & Environmental Science*, 2013, **6**, 835-840.
8. S. H. Chang, M. D. Lu, Y. L. Tung and H. Y. Tuan, *Acs Nano*, 2013, **7**, 9443-9451.
9. M. Caban-Acevedo, N. S. Kaiser, C. R. English, D. Liang, B. J. Thompson, H. E. Chen, K. J. Czech, J. C. Wright, R. J. Hamers and S. Jin, *Journal of the American Chemical Society*, 2014, **136**, 17163-17179.
10. B. Yang, X. Zuo, P. Chen, L. Zhou, X. Yang, H. Zhang, G. Li, M. Wu, Y. Ma, S. Jin and X. Chen, *ACS applied materials & interfaces*, 2015, **7**, 137-143.
11. J. Y. Lin, C. Y. Chan and S. W. Chou, *Chemical communications*, 2013, **49**, 1440-1442.
12. W. J. Ke, G. J. Fang, H. Tao, P. L. Qin, J. Wang, H. W. Lei, Q. Liu and X. Z. Zhao, *Acs Applied Materials & Interfaces*, 2014, **6**, 5525-5530.
13. Y. P. Liao, K. Pan, Q. J. Pan, G. F. Wang, W. Zhou and H. G. Fu, *Nanoscale*, 2015, **7**, 1623-1626.
14. I. A. Ji, H. M. Choi and J. H. Bang, *Materials Letters*, 2014, **123**, 51-54.
15. Z. Q. Li, F. Gong, G. Zhou and Z. S. Wang, *Journal of Physical Chemistry C*, 2013, **117**, 6561-6566.
16. H. J. Zhang, L. T. Yang, Z. Liu, M. Ge, Z. Zhou, W. Chen, Q. Z. Li and L. Liu, *Journal of Materials Chemistry*, 2012, **22**, 18572-18577.
17. M. Caban-Acevedo, M. S. Faber, Y. Tan, R. J. Hamers and S. Jin, *Nano letters*, 2012, **12**, 1977-1982.
18. M. Cabán-Acevedo, D. Liang, K. S. Chew, J. P. DeGrave, N. S. Kaiser and S. Jin, *Acs Nano*, 2013, **7**, 1731-1739.
19. S. Shukla, N. H. Loc, P. P. Boix, T. M. Koh, R. R. Prabhakar, H. K. Mulmudi, J. Zhang, S. Chen, C. F. Ng, C. H. A. Huan, N. Mathews, T. Sritharan and Q. H. Xiong, *Acs Nano*, 2014, **8**, 10597-10605.
20. Y. Y. Duan, Q. W. Tang, J. Liu, B. L. He and L. M. Yu, *Angewandte Chemie-International Edition*, 2014, **53**, 14569-14574.
21. F. Gong, H. Wang, X. Xu, G. Zhou and Z. S. Wang, *Journal of the American Chemical Society*, 2012, **134**, 10953-10958.
22. M. Wu, X. Lin, T. Wang, J. Qiu and T. Ma, *Energy & Environmental Science*, 2011, **4**, 2308-2315.
23. M.-N. Lu, C.-S. Dai, S.-Y. Tai, T.-W. Lin and J.-Y. Lin, *Journal of Power Sources*, 2014, **270**, 499-505.
24. X. Chen, J. W. Guo, Y. Hou, Y. H. Li, S. Yang, L. R. Zheng, B. Zhang, X. H. Yang and H. G. Yang, *RSC Adv.*, 2015, **5**, 8307-8310.
25. L. Kavan, P. Liska, S. M. Zakeeruddin and M. Gratzel, *Acs Applied Materials & Interfaces*, 2014, **6**, 22343-22350.
26. J. W. Guo, B. Zhang, Y. Hou, S. Yang, X. H. Yang and H. G. Yang, *J. Mater. Chem. A*, 2013, **1**, 1982-1986.
27. M. Wu, X. Lin, Y. Wang, L. Wang, W. Guo, D. Qi, X. Peng, A. Hagfeldt, M. Gratzel and T. Ma, *Journal of the American Chemical Society*, 2012, **134**, 3419-3428.
28. H. S. Chen, S. J. Lue, Y. L. Tung, K. W. Cheng, F. Y. Huang and K. C. Ho, *Journal of Power Sources*, 2011, **196**, 4162-4172.
29. A. Hung, J. Muscat, I. Yarovsky and S. P. Russo, *Surface Science*, 2002, **520**, 111-119.
30. Y. Hou, D. Wang, X. H. Yang, W. Q. Fang, B. Zhang, H. F. Wang, G. Z. Lu, P. Hu, H. J. Zhao and H. G. Yang, *Nature communications*, 2013, **4**, 1583.
31. B. Zhang, D. Wang, Y. Hou, S. Yang, X. H. Yang, J. H. Zhong, J. Liu, H. F. Wang, P. Hu, H. J. Zhao and H. G. Yang, *Scientific reports*, 2013, **3**, 1836.
32. Y. Xing, X. Zheng, Y. Wu, M. Li, W. H. Zhang and C. Li, *Chemical communications*, 2015, **51**, 8146-8149.